Dalton Transactions

PAPER

View Article Online
View Journal | View Issue

Cite this: *Dalton Trans.*, 2018, **47**, 10775

Covalently linking $CuInS_2$ quantum dots with a Re catalyst by click reaction for photocatalytic CO_2 reduction†

Jing Huang,[a] Mélina Gilbert Gatty,[a] Bo Xu,[a] Palas Baran Pati,[a] Ahmed S. Etman,[b] Lei Tian,[a] Junliang Sun,[b] Leif Hammarström[a] and Haining Tian *[a]

Covalently linking photosensitizers and catalysts in an inorganic–organic hybrid photocatalytic system is beneficial for efficient electron transfer between these components. However, general and straightforward methods to covalently attach molecular catalysts on the surface of inorganic semiconductors are rare. In this work, a classic rhenium bipyridine complex (Re catalyst) has been successfully covalently linked to the low toxicity $CuInS_2$ quantum dots (QDs) by click reaction for photocatalytic CO_2 reduction. Covalent bonding between the $CuInS_2$ QDs and the Re catalyst in the QD–Re hybrid system is confirmed by UV-visible absorption spectroscopy, Fourier-transform infrared spectroscopy and energy-dispersive X-ray measurements. Time-correlated single photon counting and ultrafast time-resolved infrared spectroscopy provide evidence for rapid photo-induced electron transfer from the QDs to the Re catalyst. Upon photo-excitation of the QDs, the singly reduced Re catalyst is formed within 300 fs. Notably, the amount of reduced Re in the linked hybrid system is more than that in a sample where the QDs and the Re catalyst are simply mixed, suggesting that the covalent linkage between the $CuInS_2$ QDs and the Re catalyst indeed facilitates electron transfer from the QDs to the Re catalyst. Such an ultrafast electron transfer in the covalently linked $CuInS_2$ QD–Re hybrid system leads to enhanced photocatalytic activity for CO_2 reduction, as compared to the conventional mixture of the QDs and the Re catalyst.

Received 24th April 2018,
Accepted 5th July 2018

DOI: 10.1039/c8dt01631c

rsc.li/dalton

Introduction

As a part of artificial photosynthesis, photocatalytic reduction of CO_2 has gained substantial interest, since it is a green method to convert solar energy and the greenhouse gas CO_2 into chemical feedstock.[1–4] Until now, there were mainly three kinds of catalysts for CO_2 photoreduction: semiconductors and metals,[5–9] synthetic molecular catalysts[10–14] and enzymes.[15–18] Though enzymes display high turnover efficiency and good selectivity, the range of possible operative conditions is restricted, which greatly limits their large-scale use. Semiconductors and metals can photo-catalyze CO_2 reduction with good stability and high activity;[19,20] however, they always suffer from poor product selectivity.[5–7,9] For example, a mixture of CO, CH_4 and C_2H_6 was produced from CO_2 by PbS nanoparticles loaded with a Cu co-catalyst.[21] In contrast, synthetic molecular catalysts often exhibit excellent selectivity, for example photoreduction of CO_2 by rhenium (Re) based catalysts normally produces only CO.[22,23] However, inefficient absorption of visible light restrains their overall photocatalytic performance, and a combination with photosensitizers is usually needed to enhance their activity. There is numerous work to broaden the photoactive region of molecular catalysts by linking them with molecular photosensitizers, such as the synthesis of supramolecular photocatalysts with ruthenium (Ru) dyes as photosensitizers and Re or Ru complexes as catalysts bridged by different ligands,[2,24–27] dyads with metalloporphyrins covalently tethered to rhenium complexes,[28–30] and other systems with organic dyes coupled to molecular catalysts.[31,32] However, molecular photosensitizer-based systems always suffer the problem of onerous synthetic routes.

Colloidal quantum dots (QDs), a kind of semiconductor nanoparticle with size smaller than their exciton Bohr radius, can be a suitable alternative to molecular photosensitizers for building an inorganic–organic hybrid system for photocatalysis. Firstly, because of the quantum confinement effect, their bandgap can be easily tuned by their size, to optimize their absorption of solar light.[33,34] Also, their band energy levels can

[a]*Department of Chemistry-Ångström Laboratory, Uppsala University, Box 523, SE 751 20 Uppsala, Sweden. E-mail: haining.tian@kemi.uu.se*
[b]*Department of Materials and Environmental Chemistry (MMK), Stockholm University, SE 106 91 Stockholm, Sweden*

†Electronic supplementary information (ESI) available. See DOI: 10.1039/c8dt01631c

be adjusted in a facile manner by varying the QD size,[33,34] composition,[35,36] and the capping ligand,[37,38] to increase the driving force for electron transfer from QDs to catalysts. Secondly, due to the large surface-to-volume ratio of QDs, molecular catalysts could adsorb on the QD surface, and the charge transfer reaction becomes much faster than in a case with freely diffusing catalysts, in which the charge transfer is primarily mediated by bimolecular collision.[39,40] Weiss *et al.* have recently employed $CuInS_2$ QDs as photosensitizers for FeTPP[41] and FeTMA catalysts,[42] and achieved impressive photocatalytic activity for these hybrid systems, due to ultrafast electron transfer from QDs to catalysts. Thirdly, in addition to being photosensitizers, semiconductor nanoparticles can also work as electron reservoirs for the catalyst, which can slow down charge recombination in the system and prolong the lifetime of a catalyst intermediate.[43] Last but not least, semiconductor nanoparticles can function as scaffolds for the catalysts, hindering the formation of catalyst dimers.[44]

To achieve efficient photo-induced catalysis, strong electronic coupling between QDs and catalysts is necessary to enable fast electron transfer from QDs to catalysts, and in that way, the catalyst molecules could be fed with more electrons to accomplish CO_2 reduction. Numerous studies have shown that, compared to unbound photosensitizers and catalysts, hybrid systems consisting of covalently-bound sensitizers and catalysts always show stronger electronic coupling and more efficient electron transfer, resulting in higher activity and selectivity for CO_2 reduction.[45–47] Moreover, when molecular catalysts are linked with QDs to form a hybrid superstructure, the immobilization process on substrates is also simplified. On the other hand, without covalent bonds, the original ligand on the QDs can act as a barrier that inhibits the adsorption of catalysts on the QD surface, hence, hindering electron transfer between them.[45] To date, only a few methods of covalent attachment of catalysts onto the QD surface have been reported, and most of them are based on molecular catalysts with an anchoring group, such as thiol groups[45] or phosphonate groups,[47,48] which can bind the catalyst molecules as ligands to the QD surface. However, the synthesis and purification processes of such catalysts with thiol or phosphate groups are often arduous. Hence, a synthetically simpler and more tunable approach for immobilizing catalysts on the QD surface is highly desirable.

The "click" reaction with azide–alkyne cycloaddition is an ideal reaction for covalent linkage of two molecules owing to its high selectivity, high yield and fast reaction kinetics under mild reaction conditions.[49–52] It is also suitable for covalently linking organic molecules to conductive surfaces.[53,54] In this work, we covalently linked the catalyst Re(4-azidomethyl-4′-methyl-2,2′-bipyridine)$(CO)_3Cl$ (Re catalyst) with $CuInS_2$ QDs by a copper-free click reaction, to synthesize the QD–Re hybrid system for CO_2 photoreduction. This is the first time that a molecular catalyst was attached on QDs with covalent bonds through a copper-free click reaction for photocatalytic reactions. Each reaction component was easy to prepare, which can be a demonstration for a straightforward and versatile strategy to link molecular catalysts with inorganic semiconductor nanoparticles. We also provide evidence that the photocatalytic activity of these QD–Re hybrid systems was enhanced by efficient electron transfer between the QDs and the Re catalyst due to the covalent linkage.

Experimental section

Materials

Indium acetate ($In(OAc)_3$, 99.99%), copper iodide (CuI, ≥99.5%), oleylamine (OAm, 97%), 1-octadecene (ODE, 90%), 3-mercaptopropionic acid (3-MPA, >99%), sulfur powder (S, 99.5%), *N*-(3-dimethylaminopropyl)-*N*′-ethylcarbodiimide hydrochloride (EDC, ≥99.0%), *N*-hydroxysuccinimide (NHS, 98%), dibenzocyclooctyne-amine (DBCO-amine), triethanolamine (TEOA, ≥99.0%), and dimethyl sulfoxide (DMSO) were purchased from Sigma-Aldrich. All chemicals and solvents were used as received.

Synthesis and ligand exchange of $CuInS_2$ QDs

The synthesis of $CuInS_2$ QDs was based on a reported method with minor modifications.[55] Briefly, 29 mg of $In(OAc)_3$ and 5 mg of CuI were put into a flask which contained 4 mL of ODE and 2 mL of OAm, and then the solution was purged with argon, followed by heating to 180 °C. Then 0.4 mL of sulfur precursor solution, prepared by dissolving 32 mg of sulfur powder in 1 mL of OAm, was injected into the flask, and the reaction system was kept at 180 °C for 20 min before the heater was removed. The obtained $CuInS_2$ QDs were purified by dispersing in hexane and precipitating with ethanol, and the final QDs were dispersed in 10 mL of toluene to form the $CuInS_2$ QD stock solution.

Then the original ligands on QDs were exchanged with 3-MPA through a ligand exchange reaction. Specifically, a MPA ligand solution, prepared by mixing 0.3 mL of MPA with 0.7 mL of methanol, with the pH of the solution adjusted to 10 using 38% NaOH aqueous solution, was dropped into 5 mL of $CuInS_2$ QD stock solution under strong stirring. After stirring for 40 minutes at room temperature, MPA capped QDs, which were in the lower part, were collected and purified with water and acetone, and finally dispersed in 10 mL of DMSO.

The Re catalyst was synthesized by following a reported method.[31]

Preparation of the QD–Re hybrid system

Typically, 5 mL of QD–DMSO solution, together with 5 mg of EDC and 2.9 mg of NHS dissolved in 1.5 mL of DMSO, were loaded in the flask, and then purged with argon for 15 min under stirring. The linker solution, produced by dissolving 10 mg of DBCO-amine in 1 mL of DMSO, was injected into the flask. Subsequently, 15 mg of the Re catalyst dissolving in 1 mL of DMSO was injected into the reaction system at room temperature. After stirring for 4.5 h, the reaction was stopped, and the covalently linked QD–Re hybrid system was obtained from centrifugation of the reaction solution. Finally, the QD–

Re hybrid system was dispersed in 10 ml of DMSO, forming a clear brown-yellowish solution.

CO_2 photocatalytic reduction

A 2 mL solution of the prepared sample (0.3 mM), TEOA (0.1 M) and DMSO was loaded into a 4.5 mL cuvette, and purged with Ar and CO_2 for 30 min and 25 min respectively. The sealed cuvette was then irradiated with a LED white lamp (≥420 nm, comparable light intensity to 1 sunlight in the region between 420 nm and 750 nm), for different times under stirring. The produced CO was taken out using a gas-tight syringe from the headspace, and measured by gas chromatography (GC).

Characterization

Ground-state ultraviolet-visible (UV-vis) absorption spectra were recorded on a Varian Cary 5000. The ground-state UV-vis spectrum of $CuInS_2$ QDs was obtained in aqueous solution, while the UV-vis spectra of the $CuInS_2$ QD–Re hybrid system and the Re catalyst alone were obtained in DMSO. Fluorescence spectra were obtained on a Horiba Jobin Yvon Fluorolog with an excitation wavelength of 470 nm. The setup for time-correlated single photon counting (TCSPC) measurements was the same as in our previous work,[50] with a light source of 470.4 nm and a long-pass filter to screen the photons below 640 nm. All samples were loaded in 1 cm cuvettes with DMSO as the solvent and purged with Ar prior to measurements. Fourier-transform infrared (FTIR) spectra were collected from solid pellets, prepared by mixing the sample powder with KBr, by using a Bruker IFS 66v/S FTIR spectrophotometer. GC measurements were conducted on an Agilent Technologies 490 Micro GC with Ar carrier gas, and CO_X columns were used. Calibration curves for CO were established by injecting a known amount of CO. The morphology and elemental analysis of the QD samples were explored by transmission electron microscopy (TEM, JEOL JEM-2100F) equipped with an energy dispersive X-ray (EDX) detector using an accelerating voltage of 200 kV.

Femtosecond mid-infrared transient absorption spectroscopy

The 800 nm output of a Ti:sapphire based amplifier with integrated oscillator and pump lasers (800 nm, 40 fs, 3 kHz, Libra LHE, Coherent Inc.) was split into two beams which were used to pump two TOPAS Primes coupled with frequency mixers (Light Conversion Ltd). This generates the visible pump at 520 nm and a broad mid-IR probe spectrum (2210–1825 cm^{-1}). The pump pulse energy hitting the sample was adjusted using a neutral density filter placed before the sample and was varied between 66 nJ and 830 nJ at 520 nm (spot size *ca.* 1900 μm^2). For the probe, the probe beam was split into two probe and reference beams. Detection of the probe and reference beams was done using a femtosecond transient absorption spectrometer (Helios IR, Ultrafast Systems LLC). The instrument response function for these experiments is *ca.* 300 fs. All spectra were recorded in a sealed liquid cell (Specac) consisting of two CaF_2 windows separated by a PTFE spacer of 640 μm path length. During the measurements, the samples were moved manually to minimize possible laser-induced sample damage. The solvent was DMSO in all experiments.

Results and discussion

Synthesis of the QD–Re hybrid system

In this work, the covalent linkage in the QD–Re hybrid system was realized from a copper-free click reaction between the alkyne group in the linker molecule (dibenzocyclooctyne-amine, DBCO-amine) and the azide group in the Re catalyst, as shown in Fig. 1. The mercaptopropionic acid (MPA) capped $CuInS_2$ QDs (tetragonal chalcopyrite structure, Fig. S1†), synthesized by following a literature method,[55] were firstly coupled with the linker DBCO-amine by amidation reaction through *N*-(3-dimethylaminopropyl)-*N*′-ethylcarbodiimide hydrochloride (EDC)/

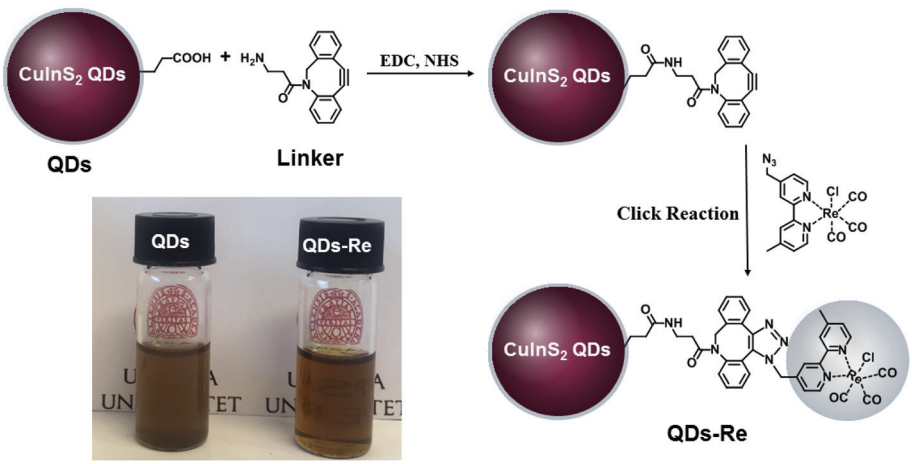

Fig. 1 Synthetic routes of the covalently-linked $CuInS_2$ QD–Re hybrid system. Insert: Photograph of $CuInS_2$ QDs and the $CuInS_2$ QD–Re hybrid system dispersed in DMSO.

N-hydroxysuccinimide (NHS) in DMSO. Subsequently, the Re catalyst functionalized with an azide group, which can quickly bind to the linker molecules on the surface of $CuInS_2$ QDs through click reaction, was added to the reaction system, by forming the $CuInS_2$ QD–Re hybrid system. All of these reactions were performed at room temperature and processed in solution, which is therefore convenient for scaling up. Before binding with the linker molecules, the MPA capped $CuInS_2$ QDs showed poor dispersibility in the organic solvent DMSO. However, after coupling with the linker and Re catalyst molecules, the DMSO solution of the $CuInS_2$ QD–Re hybrid system became much clearer, as illustrated by the insert photograph in Fig. 1. TEM images (Fig. S2†) show that, compared to MPA capped $CuInS_2$ QDs, there is no obvious change in size (7 ± 1 nm) or shape (triangle) of the $CuInS_2$ QDs after binding with the Re catalyst that could explain a better dispersibility. Thus, the improved dispersibility of the QDs in DMSO points towards a successful binding of the catalyst to the surface of the $CuInS_2$ QDs, which can increase the hydrophobicity of the QDs.

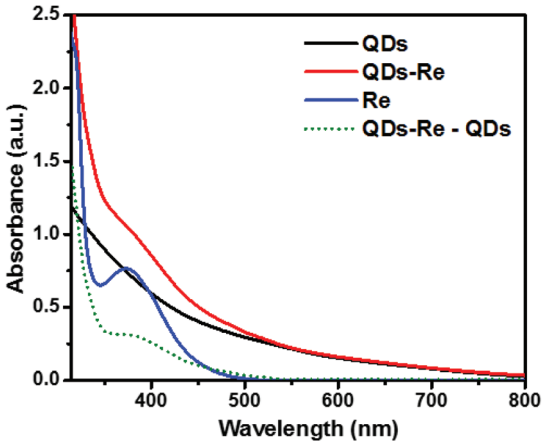

Fig. 2 UV-Vis absorption spectra of $CuInS_2$ QDs in aqueous solution, the $CuInS_2$ QD–Re hybrid system and the Re catalyst in DMSO.

Fig. 2 shows the UV-Vis ground-state absorption spectra of the $CuInS_2$ QDs, the $CuInS_2$ QD–Re hybrid system, and the Re catalysts. The as-synthesized $CuInS_2$ QDs exhibited a broad excitonic peak centered at around 540 nm with a long tail extended to 800 nm (detailed in Fig. S3†), which illustrates the fact that the $CuInS_2$ QDs can absorb the entire range of visible light up to near infrared light. The absorption of the Re catalyst began from 500 nm, and featured a maximum absorption at around 375 nm. Upon covalent binding of the Re catalyst onto the surface of $CuInS_2$ QDs, the $CuInS_2$ QD–Re hybrid system displayed absorption features both from the $CuInS_2$ QDs and the Re catalyst. The difference spectrum (the absorption spectrum of $CuInS_2$ QD–Re subtracted from that of $CuInS_2$ QDs, green dotted line in Fig. 2) resembled the absorption spectrum of the pure linker-Re catalyst, and the latter was prepared similarly to the $CuInS_2$ QD–Re hybrid system, but without $CuInS_2$ QDs in the reaction system (see in Fig. S4†). Both of them showed a slight bathochromic shift from that of the pure Re catalyst, probably due to the weaker electron withdrawing ability of the ligand. The absorption spectra confirmed the presence of the Re catalyst attached onto the $CuInS_2$ QD surface in the $CuInS_2$ QD–Re hybrid system, and the loading efficiency of catalyst molecules was about 41% (mole of the Re catalyst on per mole of $CuInS_2$ QDs) as estimated from the increase in absorbance at 375 nm compared to that of the neat QD sample.

To further confirm that the Re catalyst was attached on the QDs, Fourier-transform infrared spectroscopy (FTIR) measurements were conducted and the results are presented in Fig. 3A. The FTIR spectrum of the Re catalyst displayed three characteristic absorption peaks due to carbonyl stretches at ν_{co} = 1898, 1912 and 2021 cm^{-1}, which was in agreement with previous reports on similar $Re(bpy)(CO)_3L$ complexes.[44,56] Additionally, introduction of the azide group in the Re catalyst structure (Fig. 1) produced another absorption peak ν_{N_3} at 2110 cm^{-1}. For the $CuInS_2$ QD–Re hybrid system, the ν_{co} stretches were preserved, while the azide group stretch vanished due to the click reaction between the linker molecule and the catalyst

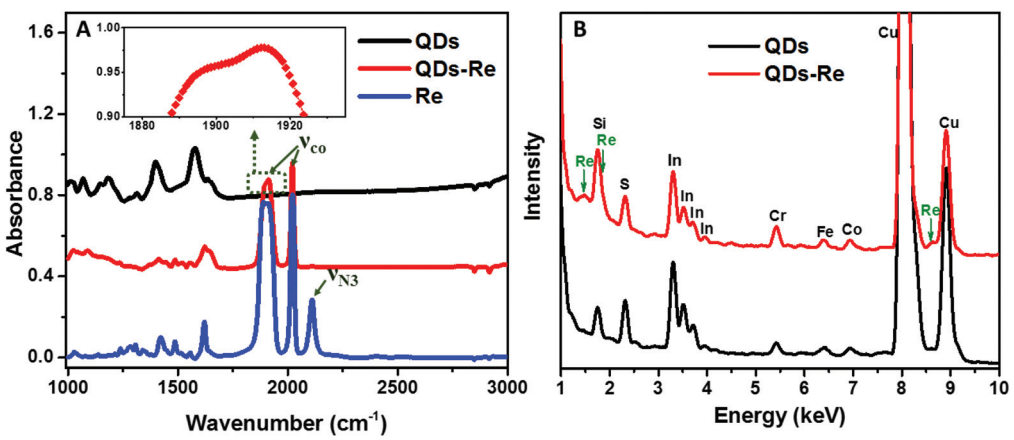

Fig. 3 (A) FTIR spectra of $CuInS_2$ QDs, $CuInS_2$ QD–Re hybrid system and the Re catalyst (inset: zoomed image of the 1875–1935 cm^{-1} region for QD–Re) and (B) EDX spectra of $CuInS_2$ QDs and the $CuInS_2$ QD–Re hybrid system.

molecule. In comparison, there were only weak ν_{CO} stretch bands for the control sample prepared without a linker molecule (Fig. S5,† sample labeled as QDsRe), implying that the Re catalysts can adsorb on the surface of QDs only to a slight extent in the absence of linker molecules. Furthermore, Re signals were detected from the $CuInS_2$ QD–Re hybrid system by energy-dispersive X-ray (EDX) measurements, as shown in Fig. 3B. Therefore, by combining the above results, we conclude that our $CuInS_2$ QD–Re hybrid system was formed through the linker assisted click reaction.

Electron transfer in the covalently-linked QD–Re hybrid system

Due to the covalent bond in the $CuInS_2$ QD–Re hybrid system, the electronic coupling between QDs and the Re catalyst is expected to be strengthened, and therefore photoinduced electron transfer (ET) from the excited QDs to the Re catalyst may occur in the hybrid system. Steady-state fluorescence spectra were first recorded for the $CuInS_2$ QDs with and without linked Re catalyst molecules, as well as the mixture solution of the $CuInS_2$ QDs and the Re catalyst (*i.e.* without a covalent bond between them) for comparison. As shown in Fig. S6,† upon excitation with 470 nm, the $CuInS_2$ QDs exhibited fluorescence around 750 nm, and the Re catalyst alone exhibited strong photoluminescence (PL) around 630 nm. After binding with the Re catalyst, the PL emission of the $CuInS_2$ QDs was almost completely quenched, while the fluorescence of the Re catalyst was retained. The retained fluorescence of Re should originate from direct excitation of a non-reduced Re catalyst. Considering that energy transfer from the QDs to the Re catalyst was energetically unfavorable (no overlap between the emission of the QDs and the absorption of the Re catalyst), the PL quenching can only be induced by charge transfer from the QDs to the linker or the Re catalyst. However, the linker alone only reduced the PL intensity to a small extent (Fig. S7†). Differential pulse voltammetry (DPV) measurement of the $CuInS_2$ QDs and cyclic voltammetry (CV) measurement of the Re catalyst (Fig. S8†) showed that their first reduction potentials were −0.99 and −0.93 V *vs.* SCE, respectively, implying that electron transfer from the QDs to the Re catalyst was energetically possible. The PL intensity of the $CuInS_2$ QDs in the mixed sample of $CuInS_2$ QDs and Re catalyst only partially decreased (Fig. S6†), as compared to the as-synthesized $CuInS_2$ QDs, which further indicated that covalent binding in the $CuInS_2$ QD–Re hybrid system enhanced the quenching of the $CuInS_2$ QD emission.

Time-correlated single photon counting (TCSPC) measurements of the $CuInS_2$ QD–Re hybrid system confirmed the accelerated decay of the fluorescence of the QDs in the presence of the Re catalyst. From the data presented in Fig. 4 and the results from biexponential fits in Table 1, we can see that the PL lifetime of QDs in the mixed solution partially decreased from that of the as-synthesized $CuInS_2$ QDs, and the decrease was mainly in the fast decay component (τ_1 = 0.587 ns (77.3%) for the mixed sample, and τ_1 = 2.39 ns (62.8%) for the as-synthesized $CuInS_2$ QDs), which was consistent with the results from steady-state fluorescence measurements. In contrast, the PL lifetime of the $CuInS_2$ QD–Re hybrid system dramatically decreased, with τ_1 = 0.243 ns (98.8%), τ_2 = 19.7 ns (1.2%), indicating that almost all the fluorescence decayed within 1 ns. The short PL lifetime of the $CuInS_2$ QD–Re hybrid system confirmed that the fluorescence of the $CuInS_2$ QDs was quenched by the covalently bound Re catalyst, and the high PL quenching yield suggested that the ET process in the system was efficient. With the average PL lifetime defined as $\langle\tau\rangle = A_1\tau_1 + A_2\tau_2$, where A_1 and A_2 are the amplitude fractions, the average lifetime for ET can be calculated according to eqn (1). The efficiency of ET is then given by eqn (2), where the latter term is equal to the ratio of the areas under the respective PL decay curve.

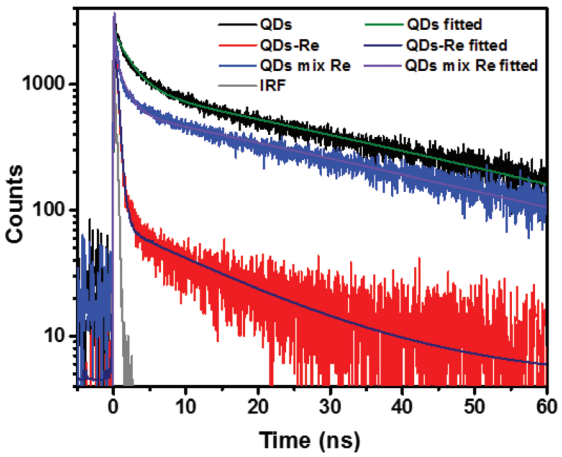

Fig. 4 Decays of the photoluminescence of $CuInS_2$ QDs, $CuInS_2$ QD–Re hybrid system, and the mixture solution of $CuInS_2$ QDs and the Re catalyst, monitored at the emission wavelengths above 640 nm, after excitation at 470 nm in DMSO. The lifetimes obtained from the fitting procedure are listed in Table 1.

Table 1 PL lifetime calculated from TCSPC measurements. The kinetics was fitted with a bi-exponential decay function[a]

Sample	QDs	QD–Re	QD–Re mixture
τ_1 (ns)	2.39 (62.8%)	0.243 (98.8%)	0.587 (77.3%)
τ_2 (ns)	36.7 (37.2%)	19.7 (1.2%)	29.9 (22.7%)
Weighted average PL lifetime $\langle\tau\rangle$ (ns)	15	0.48	7.2
χ^2/N_d	1.54	1.70	1.52

[a] Some deviations from a perfect fit (see χ^2/N_d values, and residual plots in Fig. S9) indicated that the interfacial kinetics was somewhat more heterogeneous than that described by the fit. For the purpose of the present analysis, however, a biexponential fit was still sufficient to demonstrate the large differences between the samples.

$$\frac{1}{\langle\tau_{QDs\text{-}Re}\rangle} = \frac{1}{\langle\tau_{ET}\rangle} + \frac{1}{\langle\tau_{QDs}\rangle} \quad (1)$$

$$\eta_{ET} = 1 - \frac{\langle\tau_{QDs\text{-}Re}\rangle}{\langle\tau_{QDs}\rangle} \quad (2)$$

According to eqn (1) and (2), and assuming that all PL quenching arose from electron transfer, the average ET lifetime ($\langle\tau_{ET}\rangle$) and efficiency (η_{ET}) of 0.49 ns and 97% were obtained for the QD–Re hybrid system. In other words, the majority of the electron transfer processes from $CuInS_2$ QDs to the Re catalyst occurred within 1 ns. This efficient ET process is presumably because of a strengthened electronic coupling between the $CuInS_2$ QDs and the Re catalyst, through forming the QD–Re covalent bond.[39] Note that any process faster than *ca.* 30 ps cannot be resolved by the TCSPC experiment.

In order to further investigate the origin of the PL quenching, transient absorption spectroscopy measurements in the mid-IR region were performed. The reduced rhenium should give a clear signature in the infrared region due to strong ν_{CO} stretches according to the literature.[28,57–59] Fig. S10† and Fig. 5A show the time-resolved IR (TRIR) spectra of the $CuInS_2$ QD–Re hybrid system under 520 nm excitation after subtraction of the background absorption of the conduction band electrons in the QDs. The spectra show bleaches of the ground-state CO bands of the Re catalyst at 2030, 1924, and 1897 cm^{-1}, which were slightly blue-shifted as compared to the FTIR spectrum of the QD–Re hybrid system. This blue-shift may be due to the solvent effect since the TRIR spectra were recorded in solution, while the FTIR spectra were recorded in solid samples.[44] Simultaneously, the appearance of a positive band at 2012 cm^{-1} could be observed, which is red-shifted by 18 cm^{-1} from the ground state of the CO stretching band at 2030 cm^{-1}. Numerous studies have shown that the ν_{CO} stretch bands of the one-electron-reduced species $[Re(bpy)(CO)_3Cl]^-$ normally shift to a lower energy by around 20 cm^{-1} from that of the ground state.[28,32,40,57–62] Therefore, the positive band at 2012 cm^{-1} could be assigned to the reduced form of the Re catalyst. Similar TRIR features were also observed in CdSe QD–$Re(CO)_3Cl(dcbpy)$ complexes,[40] and these results suggested that the photoinduced electrons in conduction band of QDs could effectively transfer to the Re catalyst, generating the Re catalyst anion:

$$QDs^* + Re \rightarrow QDs^+ + Re^-.$$

From Fig. 5A, we can find that the feature of the Re catalyst anion can be observed already at 300 fs after excitation, which means the electron transfer from the QDs to the Re catalyst must occur within less than 300 fs. The transient IR spectra of the Re catalyst alone recorded under the same conditions show negligible features of the Re excited state and singly reduced Re, which excludes direct excitation of the catalyst at 520 nm (Fig. S11†). Unsurprisingly, the reduced Re catalyst was also detected from the mixed sample of $CuInS_2$ QDs and Re catalyst (Fig. S12†). However, the amount of catalyst anions was less than the ones in the $CuInS_2$ QD–Re hybrid system. As shown by Fig. 5B, the signal of the reduced Re catalyst was larger in the $CuInS_2$ QD–Re hybrid system though the amount of the Re catalyst was slightly higher in the mixed sample (see the inserted comparison spectra in Fig. 5B). These results suggested that the ET process was more efficient in the covalently linked hybrid system that in the simple mixture. The signals from the reduced Re catalyst decayed with an average lifetime of ≥1.1 ns, with a significant component >5 ns (see Fig. S14 and Table S1†). Thus, the slower ET components indicated by TCSPC will not lead to an obvious rise of the reduced Re catalyst IR signal, as formation occurs concomitant with (or is slower than) its subsequent decay.

Photocatalytic activity and mechanism

The photocatalytic activity towards CO_2 reduction of our $CuInS_2$ QD–Re hybrid system was evaluated, in the presence of TEOA as an electron donor (Fig. 6). The turnover number

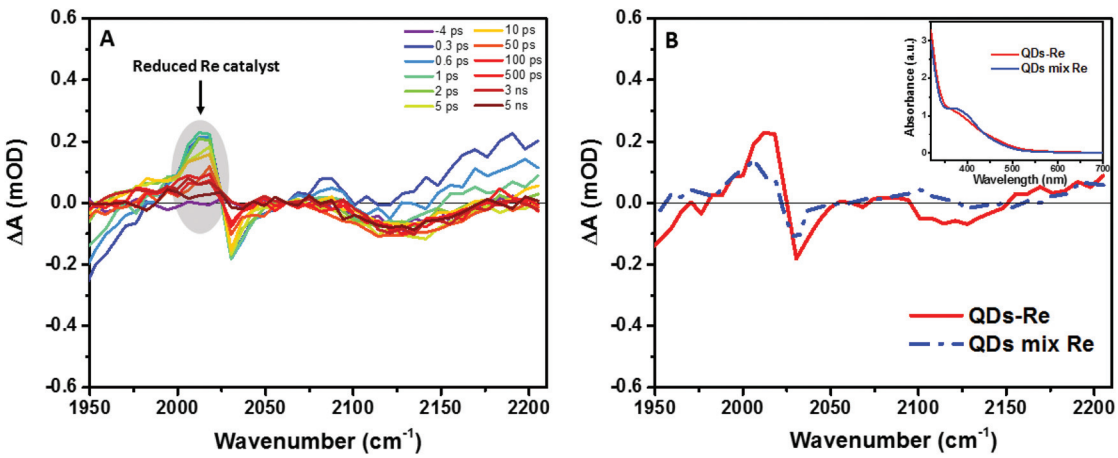

Fig. 5 (A) fs-TRIR spectra for the $CuInS_2$ QD–Re hybrid system under 520 nm excitation and (B) comparison of the fs-TRIR spectra at 1 ps for the $CuInS_2$ QD–Re hybrid system and the mixed sample of $CuInS_2$ QDs and Re catalysts. Inset: UV-Vis absorption spectra of solutions of the $CuInS_2$ QD–Re hybrid system and the mixed sample of $CuInS_2$ QDs and Re catalysts used in the fs-TRIR measurements. For the fs-TRIR spectra, the background absorption of the conduction band electrons of the QDs has been subtracted to emphasize the molecular signature of the Re catalyst. The raw data (*i.e.* before background subtraction) can be found in the ESI in Fig. S13.† The region below 1950 cm^{-1} is not shown because of the overlapping TRIR signals of the samples with absorption of the solvent (DMSO).

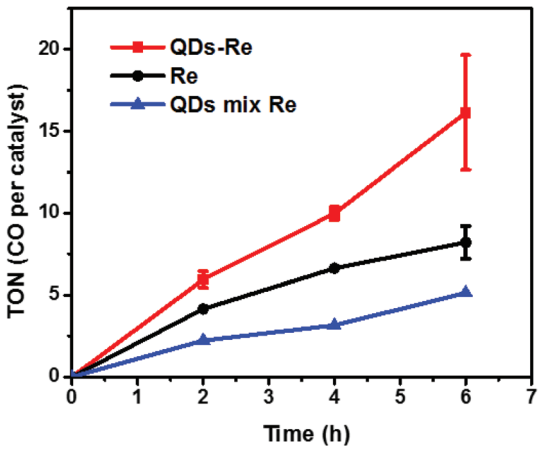

Fig. 6 Photocatalytic CO production from CO_2 (TON, error bars show ±S.D.) by the $CuInS_2$ QD-Re hybrid system, Re catalysts and the mixed sample of $CuInS_2$ QDs and Re catalysts. For photocatalytic reaction, the studied samples were dispersed in DMSO with the concentration of the catalyst fixed at 0.3 mM, and TEOA (0.1 M) was added as the electron donor. Then the samples were filled with CO_2 and illuminated using a white LED lamp.

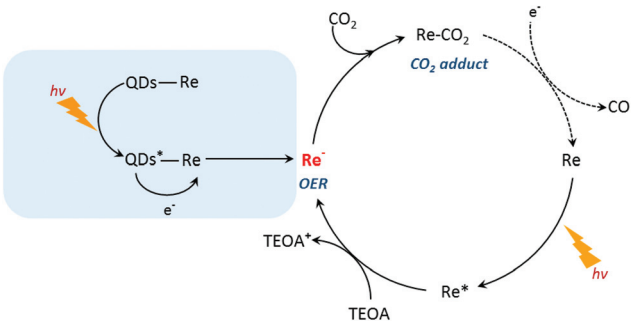

Scheme 1 Proposed photocatalytic CO_2 reduction mechanism using the $CuInS_2$ QD–Re hybrid system.

(TON), which is defined as the number of moles of CO that a mole of catalyst converts, was employed as the evaluation parameter for all samples. Control experiments conducted without either Re catalyst, TEOA, CO_2 or light, did not produce any significant amounts of CO, confirming that all these components play active roles in CO_2 reduction.

Because a LED white light (≥420 nm) was used as the light source, the Re catalyst alone exhibited moderate photocatalytic activity toward CO_2 reduction, with a TON of 8 after 6 h. No H_2 was generated from the photocatalytic system (see GC traces in Fig. S15†), which is similar to other reports.[44] When the Re catalyst was attached on the surface of the QDs in the $CuInS_2$ QD–Re hybrid system, the TON of CO by the catalyst was significantly enhanced to 16 after 6 h of photocatalysis. In contrast, in the mixed solution of QDs and Re catalyst, the QDs inhibited the activity of the catalyst, presumably by parasitic light absorption, resulting in a lower TON of 5. These results demonstrated that the linkage between QDs and the catalyst was important for the improvement of the photocatalytic activity of the catalyst, which could contribute to efficient ET from the QDs to the catalyst and then benefit the electron accumulation of the catalyst for photocatalytic CO_2 reduction. The lower TON for the mixed system compared to the Re catalyst alone can be explained by the strong visible light absorption of $CuInS_2$ QDs, which competes with the light absorption of the Re catalyst.

Based on the previous studies by Ishitani and other groups,[14,63,64] we proposed a photocatalytic mechanism of the $CuInS_2$ QD–Re hybrid system for CO_2 reduction. Without QDs, a bare Re catalyst is a classic catalyst for CO_2 reduction with high selectivity, and the photocatalytic mechanism is well studied.[14,44,65,66] As shown in Scheme 1, after absorbing light with a wavelength shorter than 500 nm, the Re catalyst can be excited, and then the excited catalyst Re* will quickly acquire an electron from the electron donor TEOA, generating one-electron reduced (OER) species of the Re complex. Notably, unlike the electro-catalysis of CO_2 reduction by the Re catalyst (Fig. S8b†),[56] the photo-induced process is conducted by the OER species of the Re complexes. The OER species play two significant roles in photocatalytic CO_2 reduction: firstly, they can bind with CO_2 in solution after ligand elimination, forming a [CO_2 adduct]; secondly, a neighboring OER species can also feed electrons to the [CO_2 adduct], converting CO_2 to CO.[14,63] When $CuInS_2$ QDs were bound to the Re catalyst, forming the $CuInS_2$ QD–Re hybrid system, the $CuInS_2$ QDs can utilize the solar light with longer wavelengths to generate electron–hole pairs. Then the photoinduced electrons in the QDs can transfer to the Re catalyst, contributing to more OER species, as proved by the TRIR results, and the QDs can subsequently be regenerated by TEOA. In the QD–Re hybrid system, the average lifetime of OER, *i.e.* the reduced Re catalyst, was ≥1.1 ns (τ_1 = 20.4 ps (54%), τ_2 = 994 ps (31%), τ_3 > 5 ns (15%), Fig. S12 and Table S1†), which is long enough to feed electrons to the [CO_2 adduct] and reduce CO_2. Compared to an unsensitized Re catalyst, there is an additional channel for the formation of OER species in the $CuInS_2$ QD–Re hybrid system; therefore, the photocatalytic activity of the $CuInS_2$ QD–Re hybrid system was improved.

Conclusions

In summary, the Re catalyst was successfully linked to $CuInS_2$ QDs by covalent bonds formed *via* a copper-free click reaction. The formation of the linked system has been confirmed by UV-Vis, FTIR and EDX measurements. The electron transfer studies have been carried out by steady-state and time-resolved fluorescence spectroscopy methods, and femtosecond transient absorption in the mid-IR region. From this study, we concluded that a fast electron transfer from the QDs to the Re catalyst occurred in the $CuInS_2$ QD–Re hybrid system, which stimulated the generation of reduced Re species, and thus improved the photocatalytic performance of the Re catalyst.

After full optimization of the hybrid system, we aim to immobilize the QD–Re system on NiO electrodes to fabricate a photocathode for CO_2 reduction.

Conflicts of interest

The authors declare no competing financial interest.

Acknowledgements

This work was supported by the Göran Gustafsson Foundation, the Olle Engkvist Byggmästare Foundation, the Swedish Research Council and the Swedish Energy Agency. Lei Tian also thanks the support from the China Scholarship Council. We extend our special thanks to Jens Föhlinger (Uppsala University) for his kind help in calculating the lifetime of the reduced Re catalyst and many helpful comments to this work. Many thanks go to Rui Sun (Uppsala University) for her great help in XRD measurement. We also thank Dr Nicolas Queyriaux, Ben Johnson, and Professor Sascha Ott (Uppsala University) for their kind help and support in GC measurements. Great gratitude also goes to Prof. Xinhua Zhong and Zhenxiao Pan (South China Agricultural University,) for their valuable advice on the synthesis of $CuInS_2$ QDs.

References

1 X. Chang, T. Wang and J. Gong, *Energy Environ. Sci.*, 2016, **9**, 2177–2196.
2 G. Sahara and O. Ishitani, *Inorg. Chem.*, 2015, **54**, 5096–5104.
3 W.-H. Wang, Y. Himeda, J. T. Muckerman, G. F. Manbeck and E. Fujita, *Chem. Rev.*, 2015, **115**, 12936–12973.
4 J. L. White, M. F. Baruch, J. E. Pander, Y. Hu, I. C. Fortmeyer, J. E. Park, T. Zhang, K. Liao, J. Gu, Y. Yan, T. W. Shaw, E. Abelev and A. B. Bocarsly, *Chem. Rev.*, 2015, **115**, 12888–12935.
5 S. Wang, B. Y. Guan, Y. Lu and X. W. D. Lou, *J. Am. Chem. Soc.*, 2017, **139**, 17305–17308.
6 B. Aurian-Blajeni, M. Halmann and J. Manassen, *Sol. Energy*, 1980, **25**, 165–170.
7 S. C. Roy, O. K. Varghese, M. Paulose and C. A. Grimes, *ACS Nano*, 2010, **4**, 1259–1278.
8 X. Jiao, Z. Chen, X. Li, Y. Sun, S. Gao, W. Yan, C. Wang, Q. Zhang, Y. Lin, Y. Luo and Y. Xie, *J. Am. Chem. Soc.*, 2017, **139**, 7586–7594.
9 K. P. Kuhl, T. Hatsukade, E. R. Cave, D. N. Abram, J. Kibsgaard and T. F. Jaramillo, *J. Am. Chem. Soc.*, 2014, **136**, 14107–14113.
10 C. Costentin, S. Drouet, M. Robert and J.-M. Savéant, *Science*, 2012, **338**, 90–94.
11 J. Bonin, M. Robert and M. Routier, *J. Am. Chem. Soc.*, 2014, **136**, 16768–16771.
12 J. D. Froehlich and C. P. Kubiak, *J. Am. Chem. Soc.*, 2015, **137**, 3565–3573.
13 H. Takeda, C. Cometto, O. Ishitani and M. Robert, *ACS Catal.*, 2017, **7**, 70–88.
14 H. Takeda, K. Koike, H. Inoue and O. Ishitani, *J. Am. Chem. Soc.*, 2008, **130**, 2023–2031.
15 B. A. Parkinson and P. F. Weaver, *Nature*, 1984, **309**, 148–149.
16 Y. S. Chaudhary, T. W. Woolerton, C. S. Allen, J. H. Warner, E. Pierce, S. W. Ragsdale and F. A. Armstrong, *Chem. Commun.*, 2012, **48**, 58–60.
17 J. Shi, Y. Jiang, Z. Jiang, X. Wang, X. Wang, S. Zhang, P. Han and C. Yang, *Chem. Soc. Rev.*, 2015, **44**, 5981–6000.
18 T. Wagner, U. Ermler and S. Shima, *Science*, 2016, **354**, 114–117.
19 Ș. Neațu, J. A. Maciá-Agulló, P. Concepción and H. Garcia, *J. Am. Chem. Soc.*, 2014, **136**, 15969–15976.
20 M. Tahir and N. S. Amin, *Appl. Catal., B*, 2015, **162**, 98–109.
21 C. Wang, R. L. Thompson, P. Ohodnicki, J. Baltrus and C. Matranga, *J. Mater. Chem.*, 2011, **21**, 13452–13457.
22 J. Hawecker, J.-M. Lehn and R. Ziessel, *J. Chem. Soc., Chem. Commun.*, 1983, 536–538.
23 T. Nakajima, Y. Tamaki, K. Ueno, E. Kato, T. Nishikawa, K. Ohkubo, Y. Yamazaki, T. Morimoto and O. Ishitani, *J. Am. Chem. Soc.*, 2016, **138**, 13818–13821.
24 Y. Tamaki, K. Koike, T. Morimoto and O. Ishitani, *J. Catal.*, 2013, **304**, 22–28.
25 Y. Tamaki, T. Morimoto, K. Koike and O. Ishitani, *Proc. Natl. Acad. Sci. U. S. A.*, 2012, **109**, 15673–15678.
26 K. Sekizawa, K. Maeda, K. Domen, K. Koike and O. Ishitani, *J. Am. Chem. Soc.*, 2013, **135**, 4596–4599.
27 Y. Kou, S. Nakatani, G. Sunagawa, Y. Tachikawa, D. Masui, T. Shimada, S. Takagi, D. A. Tryk, Y. Nabetani, H. Tachibana and H. Inoue, *J. Catal.*, 2014, **310**, 57–66.
28 C. D. Windle, M. W. George, R. N. Perutz, P. A. Summers, X. Z. Sun and A. C. Whitwood, *Chem. Sci.*, 2015, **6**, 6847–6864.
29 J. Schneider, K. Q. Vuong, J. A. Calladine, X.-Z. Sun, A. C. Whitwood, M. W. George and R. N. Perutz, *Inorg. Chem.*, 2011, **50**, 11877–11889.
30 K. Kiyosawa, N. Shiraishi, T. Shimada, D. Masui, H. Tachibana, S. Takagi, O. Ishitani, D. A. Tryk and H. Inoue, *J. Phys. Chem. C*, 2009, **113**, 11667–11673.
31 G. A. Andrade, A. J. Pistner, G. P. A. Yap, D. A. Lutterman and J. Rosenthal, *ACS Catal.*, 2013, **3**, 1685–1692.
32 J. F. Martinez, N. T. La Porte and M. R. Wasielewski, *J. Phys. Chem. C*, 2018, **122**, 2608–2617.
33 L. Brus, *J. Phys. Chem.*, 1986, **90**, 2555–2560.
34 W. W. Yu, L. Qu, W. Guo and X. Peng, *Chem. Mater.*, 2003, **15**, 2854–2860.
35 X. Zhong, M. Han, Z. Dong, T. J. White and W. Knoll, *J. Am. Chem. Soc.*, 2003, **125**, 8589–8594.
36 M. D. Regulacio and M.-Y. Han, *Acc. Chem. Res.*, 2010, **43**, 621–630.
37 K. E. Roelofs, T. P. Brennan and S. F. Bent, *J. Phys. Chem. Lett.*, 2014, **5**, 348–360.

38 P. K. Santra, A. F. Palmstrom, J. T. Tanskanen, N. Yang and S. F. Bent, *J. Phys. Chem. C*, 2015, **119**, 2996–3005.
39 K. E. Knowles, M. Malicki and E. A. Weiss, *J. Am. Chem. Soc.*, 2012, **134**, 12470–12473.
40 J. Huang, D. Stockwell, Z. Huang, D. L. Mohler and T. Lian, *J. Am. Chem. Soc.*, 2008, **130**, 5632–5633.
41 S. Lian, M. S. Kodaimati, D. S. Dolzhnikov, R. Calzada and E. A. Weiss, *J. Am. Chem. Soc.*, 2017, **139**, 8931–8938.
42 S. Lian, M. S. Kodaimati and E. A. Weiss, *ACS Nano*, 2018, **12**, 568–575.
43 M. Abdellah, A. M. El-Zohry, L. J. Antila, C. D. Windle, E. Reisner and L. Hammarström, *J. Am. Chem. Soc.*, 2017, **139**, 1226–1232.
44 C. D. Windle, E. Pastor, A. Reynal, A. C. Whitwood, Y. Vaynzof, J. R. Durrant, R. N. Perutz and E. Reisner, *Chem. – Eur. J.*, 2015, **21**, 3746–3754.
45 M. F. Kuehnel, K. L. Orchard, K. E. Dalle and E. Reisner, *J. Am. Chem. Soc.*, 2017, **139**, 7217–7223.
46 S. Sato, T. Morikawa, S. Saeki, T. Kajino and T. Motohiro, *Angew. Chem., Int. Ed.*, 2010, **49**, 5101–5105.
47 K. Muraoka, H. Kumagai, M. Eguchi, O. Ishitani and K. Maeda, *Chem. Commun.*, 2016, **52**, 7886–7889.
48 E.-G. Ha, J.-A. Chang, S.-M. Byun, C. Pac, D.-M. Jang, J. Park and S. O. Kang, *Chem. Commun.*, 2014, **50**, 4462–4464.
49 J. C. Jewett and C. R. Bertozzi, *Chem. Soc. Rev.*, 2010, **39**, 1272–1279.
50 P. B. Pati, L. Zhang, B. Philippe, R. Fernández-Terán, S. Ahmadi, L. Tian, H. Rensmo, L. Hammarström and H. Tian, *ChemSusChem*, 2017, **10**, 2480–2495.
51 N. Kaeffer, J. Massin, C. Lebrun, O. Renault, M. Chavarot-Kerlidou and V. Artero, *J. Am. Chem. Soc.*, 2016, **138**, 12308–12311.
52 E. S. Andreiadis, P.-A. Jacques, P. D. Tran, A. Leyris, M. Chavarot-Kerlidou, B. Jousselme, M. Matheron, J. Pécaut, S. Palacin, M. Fontecave and V. Artero, *Nat. Chem.*, 2013, **5**, 48–53.
53 S. A. Yao, R. E. Ruther, L. Zhang, R. A. Franking, R. J. Hamers and J. F. Berry, *J. Am. Chem. Soc.*, 2012, **134**, 15632–15635.
54 Y. Chen, H. Chen and H. Tian, *Chem. Commun.*, 2015, **51**, 11508–11511.
55 Z. Pan, I. Mora-Seró, Q. Shen, H. Zhang, Y. Li, K. Zhao, J. Wang, X. Zhong and J. Bisquert, *J. Am. Chem. Soc.*, 2014, **136**, 9203–9210.
56 M. D. Sampson, J. D. Froehlich, J. M. Smieja, E. E. Benson, I. D. Sharp and C. P. Kubiak, *Energy Environ. Sci.*, 2013, **6**, 3748–3755.
57 J. M. Smieja and C. P. Kubiak, *Inorg. Chem.*, 2010, **49**, 9283–9289.
58 A. Gabrielsson, F. Hartl, H. Zhang, J. R. Lindsay Smith, M. Towrie, A. Vlček and R. N. Perutz, *J. Am. Chem. Soc.*, 2006, **128**, 4253–4266.
59 K. Koike, D. C. Grills, Y. Tamaki, E. Fujita, K. Okubo, Y. Yamazaki, M. Saigo, T. Mukuta, K. Onda and O. Ishitani, *Chem. Sci.*, 2018, **9**, 2961–2974.
60 G. J. Stor, F. Hartl, J. W. M. van Outersterp and D. J. Stufkens, *Organometallics*, 1995, **14**, 1115–1131.
61 O. Ishitani, M. W. George, T. Ibusuki, F. P. A. Johnson, K. Koike, K. Nozaki, C. Pac, J. J. Turner and J. R. Westwell, *Inorg. Chem.*, 1994, **33**, 4712–4717.
62 N. T. La Porte, J. F. Martinez, S. Hedstrom, B. Rudshteyn, B. T. Phelan, C. M. Mauck, R. M. Young, V. S. Batista and M. R. Wasielewski, *Chem. Sci.*, 2017, **8**, 3821–3831.
63 Y. Kou, Y. Nabetani, D. Masui, T. Shimada, S. Takagi, H. Tachibana and H. Inoue, *J. Am. Chem. Soc.*, 2014, **136**, 6021–6030.
64 Y. Hayashi, S. Kita, B. S. Brunschwig and E. Fujita, *J. Am. Chem. Soc.*, 2003, **125**, 11976–11987.
65 T. Morimoto, T. Nakajima, S. Sawa, R. Nakanishi, D. Imori and O. Ishitani, *J. Am. Chem. Soc.*, 2013, **135**, 16825–16828.
66 C. Kutal, M. A. Weber, G. Ferraudi and D. Geiger, *Organometallics*, 1985, **4**, 2161–2166.